Development and Evaluation of Robot-Assisted Ultrasound Navigation System for Pedicle Screw Placement: An Ex-vivo Animal Validation

Ruixuan Li[1*], Ayoob Davoodi[1], Yuyu Cai[1], Gianni Borghesan[1,2], Nicola Cavalcanti[3], Christoph J. Laux[4], Mazda Farshad[4], Fabio Carrillo[3], Philipp Fürnstahl[3] and Emmanuel Vander Poorten[1]

[1*]Robot-Assisted Surgery group, Department of Mechanical Engineering , KU Leuven, Leuven, Belgium.
[2]Flanders Make@KULeuven, Leuven, Belgium.
[3]Research in Orthopedic Computer Science, University Hospital Balgrist, University of Zurich, Zurich, Switzerland .
[4]University Spine Center Zurich, Balgrist University Hospital, University of Zurich, Zurich, Switzerland.

*Corresponding author(s). E-mail(s): ruixuan.li@kuleuven.be;
Contributing authors: ayoob.davoodi@kuleuven.be;
yuyu.cai@kuleuven.be; gianni.borghesan@kuleuven.be;
nicola.cavalcanti@balgrist.ch; christoph.laux@balgrist.ch;
mazda.farshad@balgrist.ch; fabio.carrillo@balgrist.ch;
philipp.fuernstahl@balgrist.ch;
emmanuel.vanderpoorten@kuleuven.be;

Abstract

Purpose: Spinal instrumentation with pedicle screw placement (PSP) is an important surgical technique for spinal diseases. Accurate screw trajectory is a prerequisite for PSP. Ultrasound (US) imaging with robot-assisted system forms a non-radiative alternative to provide precise screw trajectory. This study reports on the development and assessment of US navigation for this application.

Methods: A robot-assisted US reconstruction was proposed and an automatic CT-to-US registration algorithm was investigated, allowing the registration of screw trajectories. Experiments were conducted on ex-vivo lamb spines to evaluate system performance. **Results:** In total, **72** screw trajectories are measured, displaying an average position accuracy of $\mathbf{2.80 \pm 1.14}$ mm and orientation accuracy of $\mathbf{1.38 \pm 0.61}°$. **Conclusion:** The experimental results demonstrate the feasibility of proposed US system. This work, although restricted to laboratory settings, encourages further exploration of the potential of this technology in clinical practice.

Keywords: pedicle screw trajectory, robot-assisted surgery, registration, ultrasound navigation, optical navigation

1 Introduction

Spinal instrumentation with pedicle screw placement (PSP) is an important deployed procedure in the surgical treatment of symptomatic spinal disease. However, inserting a pedicle screw is a difficult procedure. Inaccurate screw placement may damage the spinal cord or the peripheral nervous system [1]. Clinical studies have reported that between 10% and 40% of screws are misplaced more than 2 mm away from their target position [2]. Obtaining an accurate screw trajectory remains a clinical challenge, requiring significant surgical expertise and incorrectly placed screws impose an avoidable and non-negligible burden on patients and our healthcare system.

The development of intraoperative navigation techniques has facilitated the evolution of robot-assisted spine surgery. With computer-assisted navigation, a surgeon is able to localize the screw trajectory on a 3D anatomic structure hidden below the patient skin. Medical imaging modalities, such as fluoroscopy, could be employed to assist PSP intraoperatively [3, 4]. The free hand fluoroscopy navigation system achieves a 1.83 ± 1.49 mm position and $1.23 \pm 1.25°$ rotation accuracy with a guide template [5]. However, fluoroscopy has ionizing radiation and leads to longer operating times as its use interrupts the operation flow. Consequently, non-radiation alternatives, such as optical and ultrasound (US) navigation, are being explored to provide accurate guidance for screw placement.

The integration of computer-assisted navigation with modern robot platforms is being considered for enhancing spine surgery [6]. Several studies on robot-assisted optical navigation have been elaborated over the years. Smith *et al.* implemented a camera-based robot-assistive system for polyaxial PSP [7]. The accuracies with the entry point and the destination point of screw trajectories were obtained at 0.49 ± 0.17 mm and 1.49 ± 0.46 mm, respectively, on a synthetic phantom. Several commercial systems were designed for spine surgery, such as the ROSA (Zimmer Biomet, Warsaw, IN) and the Excelsius GPS (Globus Medical, Inc., Audubon, PA). In studies, the preoperative surgical plan was registered to the robot frame to guide the screw placement. Experiments reported an entry point accuracy of 2.05 ± 1.20 mm to 2.30 ± 1.60 mm on both ex-vivo and in-vivo humans [8, 9]. With optical navigation, registration accuracies of preoperative model and surgical plans were close to 1.3 ± 0.1 mm [10].

However, using reference markers leads to extra trauma to the patient. Optical systems also suffer from line-of-sight and marker overlap problems.

The use of US navigation has been proposed to avoid intraoperative radiation and the need for extra markers on the patient's skin. However, the performance of the US navigation is influenced by the limited 2D scans, which can hardly cover all potential examination regions. It is necessary to reconstruct the vertebrae surfaces from 2D images to 3D space. With such a system, the screw trajectories could be registered without requiring additional radiation and incisions on the patient. Previous studies have been implemented to evaluate US navigation performance [11, 12]. For instance, Ottacher *et al.* reported free-hand US approach to reconstruct the 3D vertebra anatomy for PSP, achieving 0.8 ± 0.6 mm position accuracy on synthetic models [11]. Similarly, Chan *et al.* also implemented a US navigation system to identify the screw trajectory for free-hand PSP [12]. The US-reconstructed vertebral surfaces were used by registering with the preoperative CT model to localise the target bone and implement the preoperative surgical plan. The average accuracy of the screw trajectory was 0.4 ± 0.4 mm and $2.1 \pm 0.9°$ over 684 trials. However, this work was only manual conducted on a synthetic experiment phantom.

Whereas, around 80–90.5% of sonographers report work-related musculoskeletal conditions in the upper neck and back, caused by the repetitive and prolonged nature of manual ultrasonography [13]. Thus, the robot-assisted system could be used for acquiring a US scan and avoiding performance influenced by US visualisation skills and fatigue. The control ability of robotic system could be improved to 34.14 times higher than that of manual scanning while maintaining good US image quality [14].

To better serve the PSP procedures, a few studies have investigated the use of intraoperative US navigation for robot-assisted PSP. In previous work [15], We have developed a robot-assisted US system to reconstruct the 3D spinal anatomy for spine surgery. This paper extends that study to develop a non-radiation robot-assisted US system to provide intraoperative screw trajectories for PSP. This work also implements a 3D US reconstruction framework with BCDU-net segmentation network [16]. An automatic CT-US registration approach is investigated to provide the intraoperative surgical plan without manual initialization. Furthermore, a validation is performed on ex-vivo lamb spines using the proposed robot-assisted US navigation system.

The rest of the paper is organized as follows: section 2 describes the methods for this study, including the robotic US reconstruction and details on the registration procedures. section 3 details the experimental design and results on the ex-vivo lamb spines. section 4 and section 5 contain detailed discussions and insights from the experimental results.

2 Materials and Methods

The proposed system consists of two tasks that need to be fulfilled, namely US reconstruction and CT-US registration, as shown in fig. 1. Firstly, section 2.1 describes a deep learning-based bone segmentation and 3D reconstruction approach. Then, an automatic CT to 3D US registration approach is demonstrated in section 2.2. Finally, section 2.3 introduces the experimental setup and phantoms.

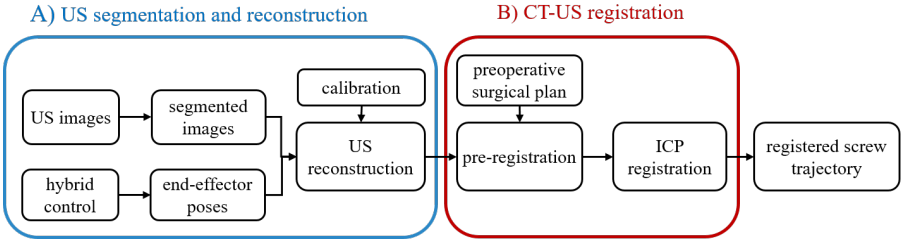

Fig. 1 Workflow of the proposed US navigation-based robot-assisted PSP, containing A) the US reconstruction and B) automatic registration workflows. After the US reconstruction and registration activities are successfully executed, the preoperative screw trajectories can be expressed in the robot base frame and thus can be executed autonomously by the robotic system.

2.1 US segmentation and reconstruction

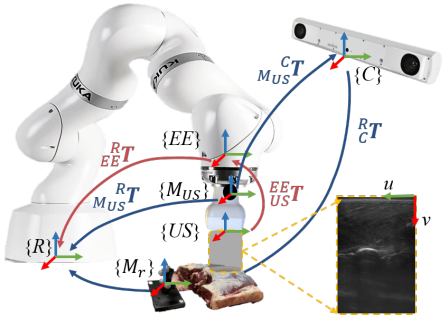

Fig. 2 Overview of the coordinate frames and transformation matrices used in this study. The notation ${}^{A}_{B}\boldsymbol{T}$ denotes the transformation from frame {B} to frame {A}. The transformations in red are used for 3D reconstruction in the robot base frame, while the transformations in blue are employed for validation by using the optical navigation system. u and v are the US image coordinates in pixels.

Before the experiment, spatial and temporal calibrations need to be performed with a Z phantom, as described in [17]. A spatial calibration is done to derive the homogeneous transformation matrix from the US image frame to the robot end effector frame. The temporal calibration compensates for the temporal offset between the measured poses of the robot end effector and the corresponding poses from the recorded US images.

A robotic scanning approach using a hybrid (i.e., position and force) control strategy is performed to acquire US images, as introduced in [15]. The spatial relationships between the different frames are shown in fig. 2. During scanning, the contact force between the US probe and skin is kept constant at 5 N. Several predefined points are selected on the skin surface with admittance control to teach an appropriate scanning trajectory that is then executed automatically.

The US reconstruction aims to reconstruct the 3D surface meshes from the anatomic features in the 2D US images. A deep learning-based network segments the

US images and extracts the edges of different anatomy at the pixel level, as shown in fig. 3. The bone contours are automatically extracted using deep learning-based image processing, BCDU-Net. BCDU-Net extends the traditional U-Net [18] with bidirectional convolutional layers allowing information to flow through the network and reuse features. For training, 200 images are manually collected from a lamb spine, which is excluded from the experiment. The recorded images are manually labelled by the operators and augmented to 600 images with left-right flip and random rotation. Subsequently, the images are cropped as 480×480 pixels. Then, the pre-processed images are fed into the network. The model is trained for 20 epochs with a $1e^{-4}$ learning rate. The same dataset is also fed to the U-Net to provide a baseline for comparison. The architecture is described in our previous work [15]. After segmentation, the images are processed with thresholding and a morphological operator. The Canny edge detection extracts the bone contours from the processed images.

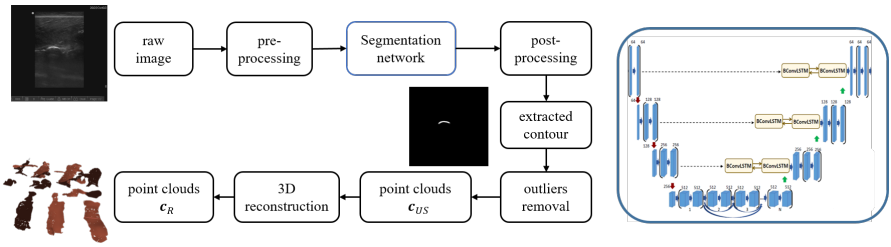

Fig. 3 Block schema of the image-processing pipeline for automatic bone contour extraction and reconstruction.

Subsequently, the segmented 2D US images are reconstructed with the proposed approaches in our previous work [15]. Each pixel $\boldsymbol{c}_{US}$ is represented in the robot base frame $\{R\}$ by the following equation:

$$\boldsymbol{c}_R = {}^{R}_{EE}\boldsymbol{T}\ {}^{EE}_{US}\boldsymbol{T}\ \boldsymbol{T}_s\ \boldsymbol{c}_{US} \tag{1}$$

where ${}^{R}_{EE}\boldsymbol{T}$ presents the transformation from the end effector $\{EE\}$ to the robot base by the robot's forward kinematics. The transformation between the US image frame $\{US\}$ and robot end effector ${}^{EE}_{US}\boldsymbol{T}$ and scaling factor $\boldsymbol{T}_s$ are calibrated in advance. Then, a radius outlier removal with the radius of 0.01 is applied to the generated point clouds to remove outliers. The algorithm computed the Euclidean distance to the nearest neighbours. Finally, the reconstruction model is obtained as a point cloud in the robot base frame for registration and visualization.

2.2 CT-US registration

After reconstruction, the preoperative CT model with the screw trajectories is converted from the CT frame $\{CT\}$ to the robot base frame by estimating the transformation matrix ${}^{R}_{CT}\boldsymbol{T}$. To date, the iterative closest point algorithm (ICP) is the most widely used registration method in computer-assisted systems. However, for this application, ICP tends to converge in local minima, as the vertebrae are highly similar to each other and symmetric [19]. Thus, a more elaborated approach, as shown in fig. 4,

is adopted. To conduct the 3D registrations, the CT model is converted to the same resolution as our 3D reconstruction model by down-sampling the point clouds. The CT model is then aligned with the reconstructed model, which is already conveniently expressed in the robot base frame.

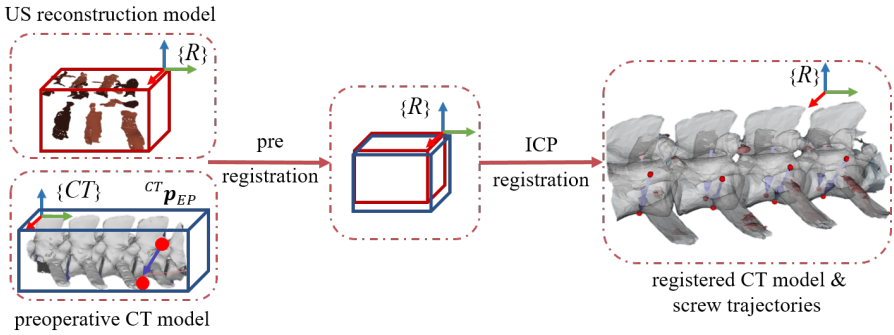

Fig. 4 Flowchart of automatic registration including pre-registration and ICP registration. The preoperative CT model $\{CT\}$ and screw trajectories ${}^{CT}\boldsymbol{p}_{EP}$ are registered with the 3D reconstructed US model $\{US\}$ in the robot base frame $\{R\}$.

The first step is performed to provide a rough initialization in proximity and orientation for the next step to avoid the local minima. Two 3D bounding boxes are generated around the reconstruction model and the preoperative CT model. Then the centre point and three intersecting points between the axes and bounding box surfaces are identified as landmarks. The point-to-point registration is applied to match the corresponding points on the two 3D point clouds. Then, the transformation to register the models is found and applied to the preregistered CT model. Second, the ICP [20] registration algorithm is applied to fine-tune the registration automatically. Finally, the registration error is computed. The decision to iterate is made based on whether the average surface distance has decreased to the target threshold of 0.1 mm. The preoperative CT model and predefined screw trajectories ${}^{CT}\boldsymbol{p}_{EP}$ are then transformed into the robot base frame ${}^{R}\boldsymbol{p}'_{EP}$ by:

$$ {}^{R}\boldsymbol{p}'_{EP} = {}^{R}_{CT}\boldsymbol{T}\ {}^{CT}\boldsymbol{p}_{EP} \tag{2} $$

2.3 Experimental setup and ex-vivo phantoms

The proposed robotic US system integrates a lightweight robotic arm (KUKA LBR Med 7, Augsburg, Germany) and a US imaging system (Sonosite, FUJIFILM, USA) as shown in fig. 5. The US system uses a 7.5 MHz linear probe. The setting of US device, namely detection depth and time gain compensation (TGC), is chosen to cover the phantom with a clear image view. A custom-designed US probe holder is mounted at the robot's end effector by a fast tool changer (G-SHW063-2UE, GRIP GmbH, Germany). A frame grabber (Epiphan Systems Inc. Palo Alto, California, USA) streams the US images at 50 Hz. A 6 DoF Force Torque sensor (Nano25, ATI Industrial

Automation Inc.) connecting the US probe at the robot end-effector measured the interaction forces and torques between the US probe and the contacted tissue surface. A PC workstation (Intel Xeon Silver 4216 Processor, CPU @2.6 GHz, 64GB RAM) is used for data acquisition and processing in Ubuntu 20.04. The Open Robot Control Software (Orocos version 2.9.0 [21]) is used for robotic control middleware for real-time robot control at 200 Hz. An NVIDIA RTX A4500 and NVIDIA Compute Unified Device Architecture (CUDA) are used to accelerate image processing computations.

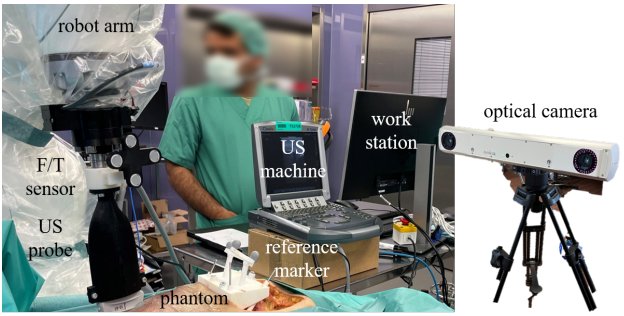

Fig. 5 Illustration of the experimental setup.

Ex-vivo lamb spines are used for qualitative and quantitative evaluation, as shown in fig. 6. Three lamb spines are separately fixed by using screws from the side to avoid motion during US scanning. The preoperative CT model of the lamb spine is segmented from 2D images by the operator using the software tool ITK-SNAP [22]. The region of interest is selected by the surgeon and saved as a rigid model for registration. For each lamb, 8 trajectories are predefined on the pedicle by the operators on the pre-operative CT model. The scanning and registration are conducted three times, resulting in 72 (8 trajectories x 3 lambs x 3 scans) screw trajectories. To assess the US navigation quality, an optical camera (FusionTrack 500, Atracsys, Switzerland) and optical markers are used to provide the ground truth for evaluation. The optical tracking system tracks the pose of the vertebrae at 50 Hz through an inserted reference marker. A second optical marker is attached to the US holder to track the probe poses.

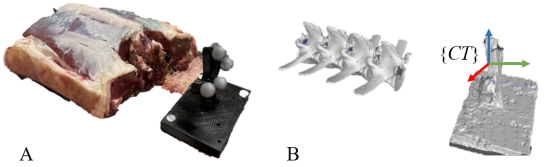

Fig. 6 An example of the ex-vivo lamb spine and optical marker for qualitatively and quantitatively experimental validation. (A) the ex-vivo lamb spine with a reference marker; (B) a preoperative CT model of the ex-vivo lamb spine and the optical marker.

3 Experiments and results

The robotic scanning was performed on three ex-vivo lamb spines to verify the effectiveness of the proposed US navigation system. The evaluation criteria and results of robot-assisted US navigation are summarized in this section. Firstly, the results of image segmentation and reconstruction are described in section 3.1. Secondly, the screw trajectory errors on lamb spines are presented in section 3.2.

3.1 Evaluation of Segmentation and Reconstruction

The BCDU-Net segmentation was evaluated with 30 testing images and compared to a U-Net segmentation. The testing images covering all the anatomic features were acquired from an ex-vivo lamb spine from the experiment. The accuracy (ACC) and F1-score (F1) metrics were used to compare the automatic segmentation results (by means of BCDU-Net and U-Net) against the manual segmentation, which was considered the ground truth. Table 1 presents the image segmentation results. BCDU-Net segmentation achieves a higher mean accuracy of 93.90%, while U-Net yields a mean accuracy of 92.85%. Besides, BCDU-Net also shows a greater mean F1 score of 71.12% compared to U-Net, which has an F1 score of 64.71%. Overall, the segmentation speed of a single image is around 15 Hz. Examples of U-Net segmentation and BCDU-Net segmentation are presented in fig. 7.

Table 1 The results of image segmentation on the testing dataset.

Model	ACC (%)	F1 (%)
U-Net	92.85	64.71
BCDU-Net	**93.90**	**71.12**

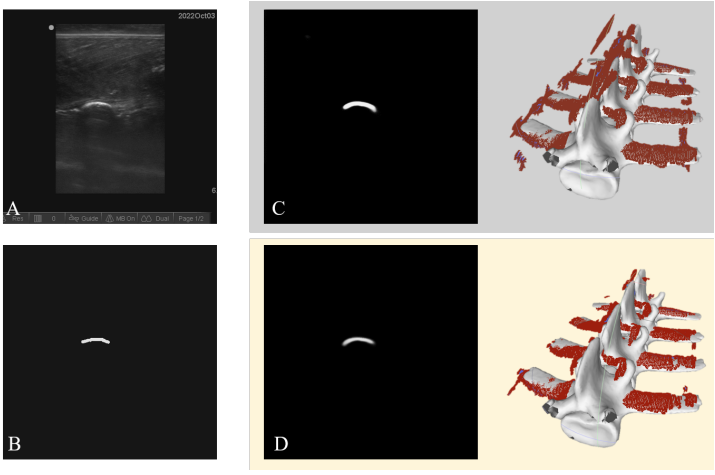

Fig. 7 Examples of the (A) raw US image and (B) manually labelled image. The segmented image and 3D US reconstruction with (C) U-Net and (D) BCDU-Net. The reconstructed model (red) is overlaid with the corresponding CT model (white).

Each lamb spine was assembled with a reference marker. The marker has an attached frame $\{M_r\}$, as shown in fig. 2. The reference marker was segmented in the CT scan along with the phantom and thus is rigidly attached to the CT frame $\{CT\}$. ${}^{C}_{M_r}\boldsymbol{T}$ represents the pose of the marker in the camera frame. Subsequently, a camera-to-robot calibration was performed as described in the previous work [23]. The proposed camera-to-robot calibration yielded a maximum 0.85 mm translation error and 1.81° rotation error.

To assess the 3D reconstruction, the CT models of the ex-vivo phantom were converted to the robot base frame by using the estimated camera-to-robot transformation ${}^{R}_{C}\boldsymbol{T}$. The average Euclidean distance between the reconstructed point clouds and the CT model was calculated as a 3D localization error to indicate the reconstruction performance. The robotic scanning was repeated three times on each lamb spine. The results were calculated and summarized in table 2. The mean localization error is computed for each lamb spine, then the overall average error and standard deviation is calculated from the mean error.

Table 2 The results of 3D reconstruction with U-Net and BCDU-Net. Measurements are in millimeters.

Model	Lamb 1	Lamb 2	Lamb 3	Mean ± Std.Dev.
U-Net	4.59±5.58	3.02±3.71	2.78±3.70	3.46±4.33
BCDU-Net	1.91±1.55	1.71±1.64	1.71±1.24	1.78±1.48

The mean 3D localization error is 1.78 ± 1.48 mm with BCDU-Net segmentation and 3.46 ± 4.33 mm with U-Net segmentation. The maximum error is 4.59 ± 5.58 mm in lamb 1 with U-Net segmentation. The results of 3D reconstruction for BCDU-Net segmentation are all within 2.00 mm among 9 scans (3 lambs x 3 scans); the point of maximum distance was typically located on the surfaces of the spinous process.

3.2 Evaluation of CT-US registration

The predefined screw trajectories in the CT frame ${}^{CT}\boldsymbol{p}_{EP}$ were converted into the robot base frame ${}^{R}\boldsymbol{p}_{EP}$ (i.e., ground truth) using the optical marker $\{M_r\}$ for evaluation.

$$ {}^{R}\boldsymbol{p}_{EP} = {}^{R}_{C}\boldsymbol{T}\ {}^{C}_{M_r}\boldsymbol{T}\ {}^{M_r}_{CT}\boldsymbol{T}\ {}^{CT}\boldsymbol{p}_{EP} \tag{3} $$

The following approach was proposed to qualify the screw trajectory's accuracy. When evaluating the system's positioning accuracy, the Z coordinate was not considered because the screw would move along the trajectory [24]. The orientation around the Z axis of the screw trajectory was also not measured since the screw was able to rotate around its Z axis. The position and orientation errors were calculated by comparing the projected screw trajectory ${}^{R}\boldsymbol{p}''_{EP}$ with the targeted trajectory ${}^{R}\boldsymbol{p}_{EP}$ obtained from optical navigation, as shown in fig. 8.

The translation error e_t was computed as the shortest 2D distance between the projected entry point from US navigation and the entry point from the optical navigation. The resultant rotation error e_r was calculated as a root sum square, as defined in the previous study [12].

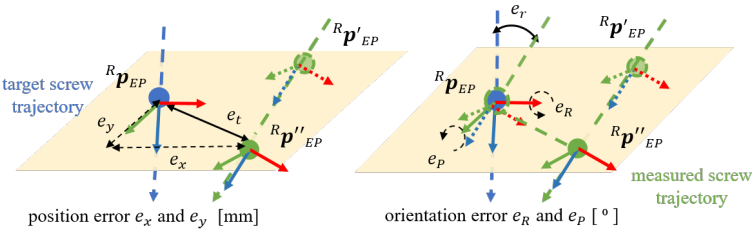

Fig. 8 Illustration of the target screw trajectory frame ${}^{R}\boldsymbol{p}_{EP}$ and the measured screw trajectory frame ${}^{R}\boldsymbol{p}''_{EP}$ in the robot base frame. e_t is the translation error, e_r is the rotation error.

$$e_t = \sqrt{({}^{R}p_{EP,x} - {}^{R}p''_{EP,x})^2 + ({}^{R}p_{EP,y} - {}^{R}p''_{EP,y})^2} \tag{4}$$

$$e_r = \sqrt{({}^{R}p_{EP,roll} - {}^{R}p''_{EP,roll})^2 + ({}^{R}p_{EP,pitch} - {}^{R}p''_{EP,pitch})^2} \tag{5}$$

Table 3 summarizes the translation and rotation errors of the 72 measured screw trajectories on ex-vivo lamb spines. With BCDU-Net segmentation, the mean translation error is 2.80 ± 1.14 mm, and the mean rotation error is $1.38 \pm 0.61°$. The maximum translation error is 2.96 ± 0.55 mm, while the maximum rotation error is $1.50 \pm 1.48°$ in lamb 3. With U-Net segmentation, the screw trajectories yield a larger translation error of 3.47 ± 1.07 mm and rotation error of $1.81 \pm 1.12°$.

Table 3 Results of the translation and rotation error of screw trajectory from US navigation compared to the optical navigation.

Model	Error	Lamb 1	Lamb 2	Lamb 3	Mean ± Std.Dev.
U-Net	e_t $[mm]$	3.64 ± 1.27	3.83 ± 0.96	2.94 ± 0.77	3.47 ± 1.07
	e_r $[°]$	1.53 ± 0.13	1.14 ± 0.57	2.78 ± 1.42	1.81 ± 1.12
BCDU-Net	e_t $[mm]$	2.88 ± 1.29	2.55 ± 1.40	2.96 ± 0.55	2.80 ± 1.14
	e_r $[°]$	1.29 ± 0.19	1.34 ± 0.92	1.50 ± 0.48	1.38 ± 0.61

4 Discussion

Inaccurate pedicle screw placement might result in a breach and permanent neurological injury to the patient. It is crucial to ensure an accurate screw trajectory with intraoperative navigation and robot-assisted systems.

Medical imaging technology, such as fluoroscopy, has increased patient safety, accuracy, and operative efficiency in pedicle screw placement procedures. This US-based approach could potentially result in a 97.8% radiation dose reduction to both patient and surgeon [25]. Optical navigation also appears to increase accuracy because of the ability to detect the real-time position of the patient. Burstromt *et al.* achieved a technical accuracy of 0.48 ± 0.44 mm, and 0.68 ± 0.58 mm at the entry point in the axial and sagittal views with a robotic guidance system [26]. However, bone pins with optical markers are still required, resulting in an extra incision on patient's back. The US-based framework provides an alternative to non-invasive navigation.

Thus, this paper proposed a non-radiative US-based navigation system for robot-assisted PSP to avoid extra trauma to the patient. Although a preoperative CT model is still required, the US navigation could significantly decrease the intraoperative radiation dose to both patients and surgeons.

4.1 US segmentation and reconstruction

Since the CT-US registration relies on the reconstructed anatomic features, an accurate US image segmentation is essential. A BCDU-Net was implemented in this work and compared to the traditional U-Net. The BCDU-Net achieves 93.90% accuracy and 71.12% F1 score. The U-net provides a lower F1 score as there are still outliers close to the spinous processes. It is found that segmentation becomes difficult when the bone is very close to the skin. For instance, the reflection of spinous processes is hard to distinguish as it is influenced by the skin-tissue reflection from the surrounding fat tissues [27].

Then, the performance of the 3D reconstruction is further investigated compared to the preoperative CT model with optical navigation. Both reconstructions present anatomical features such as transverse processes and facet joints on visual inspection. With BCDU-Net segmentation, a mean 3D localization error is 1.78 ± 1.48 mm. As a result, the mean reconstruction results with BCDU-Net segmentation outperform those from U-Net segmentation. A better image segmentation contributes to a better 3D reconstruction. The errors are smaller, with fewer outliers on the reconstructed point clouds.

With robotic scanning, the system performance has better reliability and reputability [28]. The proposed robotic system also provides a stable force control around 5 N, keeping regular contact with the skin surface compared to manual scanning [15]. The robot-assisted system achieves smooth scanning with constant speed over the complex back contour.

4.2 CT-US registration

This paper proposed an automatic CT-US registration. Compared with current approaches, our proposed method is fully automated and does not require manual

initialization, which typically takes around 8 to 10 minutes [29, 30]. This automatic registration would also eliminate the need to train operators in ultrasound landmark recognition.

The proposed system was validated with ex-vivo lamb spines for screw trajectory assessment. As a result, 72 screw trajectories were measured on three lamb spines. The mean translation accuracy is 2.80 ± 1.14 mm, and rotation accuracy is $1.38 \pm 0.61°$. Our proposed segmentation and registration approach had similar target registration accuracy to other recently reported CT-US registration methods. Wein *et al.* developed a global automatic registration and achieved a median target registration of 3.7 mm on the cadaveric femur [31]. Salehi *et al.* achieved a median registration error of 2.76 mm on the cadaveric pelvis with a deep learning-based bone segmentation [32]. Salehi *et al.* also found that the success of registration depended on the point clouds sharing a very similar point cloud representation. This makes it less suitable for human tissue where there is no guarantee that the US reconstruction would contain all anatomic bone features (i.e., vertebra body) as the CT preoperative model.

Moreover, there are also several researchers propose the automatic US to CT registration. Brößner *et al.* provided a comprehensive comparison of deep learning-based registration with validation on 3D printed carpal phantom for percutaneous scaphoid fixation [33]. With the proposed system, the screw placement achieves 1.0 ± 0.6 and 0.7 ± 0.3 mm at the distal and proximal pole, respectively.

4.3 Limitations and future work

The main limitation of this study is that the drilling procedure is excluded. This part of the procedure has been purposefully left out at this stage since it is difficult to compare the navigation accuracy, including the drilling error discerning which are the causes of accuracy loss, which is the scope of this work. For future work, the navigation performance will be evaluated with screw insertion in the lamb or human spine. Further investigations will allow comparability in clinical studies, targeting the assessment of reliability and usability and highlighting the difficulties encountered in surgery.

Furthermore, to move toward in-vivo investigation, physiological motion, such as breathing motions, must be taken into account. Moreover, the stiffness and deformations of the human spine may differ from that of a lamb. The difference in image segmentation and registration needs to be tackled before in-vivo validation can be considered.

The developed system could also be potentially used for motion tracking in minimal invasive pedicle screw placement. After reconstruction and registration, the US probe could still be placed on the patient's skin to monitor the motion of vertebrae and update it simultaneously.

5 Conclusion

This paper quantitatively evaluates the accuracy of intraoperative screw trajectory registration based on US registration on ex-vivo lamb spines compared to optical navigation supported by fiducials. Although preoperative scanning is required, this

method could potentially result in a significant decrease in the radiation dose to the patient compared to fluoroscope-based intraoperative navigation. More importantly, the result demonstrates preliminary results showing that US navigation could potentially be used to plan screw trajectories for PSP surgery with reduced trauma induced by optical markers. This work helps bridge, but not fully close, the gap toward use in clinical practice. Further investigations with conducting drilling will allow comparability in clinical studies, targeting the assessment of reliability and usability and highlighting the difficulties encountered in surgery.

Funding. This project has received funding from the European Union's Horizon 2020 research and innovation programme under grant agreement no. 101016985 (FAROS) and Flemish Research Foundation (FWO) under grant agreement no.G0A1420N (Radar-spine) and no.1S36322N (Harmony).

Conflict of interest . The authors have no conflicts of interest to declare.

Ethics approval. Not applicable.

Availability of data and materials. The datasets generated and analyzed during the current study are available from the corresponding author upon reasonable request.

ORCID. Ruixuan Li https://orcid.org/0000-0003-2882-8398

References

[1] Farshad, M., Betz, M., Farshad-Amacker, N.A., Moser, M.: Accuracy of patient-specific template-guided vs. free-hand fluoroscopically controlled pedicle screw placement in the thoracic and lumbar spine: a randomized cadaveric study. European Spine Journal **26**(3), 738–749 (2017). https://doi.org/10.1007/s00586-016-4728-5

[2] Shoham, M., Burman, M., Zehavi, E., Joskowicz, L., Batkilin, E., Kunicher, Y.: Bone-mounted miniature robot for surgical procedures: Concept and clinical applications. IEEE Transactions on Robotics and Automation **19**(5), 893–901 (2003). https://doi.org/10.1109/TRA.2003.817075

[3] Mason, A., Paulsen, R., Babuska, J.M., Rajpal, S., Burneikiene, S., Nelson, E.L., Villavicencio, A.T.: The accuracy of pedicle screw placement using intraoperative image guidance systems: a systematic review. Journal of Neurosurgery: Spine **20**(2), 196–203 (2014). https://doi.org/10.3171/2013.11.SPINE13413

[4] Gao, C., Phalen, H., Margalit, A., Ma, J.H., Ku, P.-C., Unberath, M., Taylor, R.H., Jain, A., Armand, M.: Fluoroscopy-guided robotic system for transforaminal lumbar epidural injections. IEEE Transactions on Medical Robotics and Bionics, 1–1 (2022). https://doi.org/10.1109/TMRB.2022.3196321

[5] Wu, C., Deng, J., Li, T., Tan, L., Yuan, D.: Percutaneous pedicle screw placement aided by a new drill guide template combined with fluoroscopy: an accuracy

study. Orthopaedic Surgery **12**(2), 471–479 (2020). https://doi.org/10.1111/os.12642

[6] Huang, M., Tetreault, T.A., Vaishnav, A., York, P.J., Staub, B.N.: The current state of navigation in robotic spine surgery. Annals of Translational Medicine **9**(1) (2021). https://doi.org/10.21037/atm-2020-ioi-07

[7] Smith, A.D., Chapin, J., Birinyi, P.V., Bhagvath, P.V., Hall, A.F.: Automated polyaxial screw placement using a commercial-robot-based, image-guided spine surgery system. IEEE Transactions on Medical Robotics and Bionics **3**(1), 74–84 (2021). https://doi.org/10.1109/TMRB.2020.3037339

[8] Lefranc, M., Peltier, J.: Accuracy of thoracolumbar transpedicular and vertebral body percutaneous screw placement: coupling the rosa® spine robot with intra-operative flat-panel ct guidance—a cadaver study. Journal of Robotic Surgery **9**, 331–338 (2015). https://doi.org/10.1007/s11701-015-0536-x

[9] Benech, C.A., Perez, R., Benech, F., Greeley, S.L., Crawford, N., Ledonio, C.: Navigated robotic assistance results in improved screw accuracy and positive clinical outcomes: an evaluation of the first 54 cases. Journal of Robotic Surgery **14**(3), 431–437 (2020). https://doi.org/10.1007/s11701-019-01007-z

[10] Sorriento, A., Porfido, M.B., Mazzoleni, S., Calvosa, G., Tenucci, M., Ciuti, G., Dario, P.: Optical and electromagnetic tracking systems for biomedical applications: A critical review on potentialities and limitations. IEEE reviews in biomedical engineering **13**, 212–232 (2019). https://doi.org/10.1109/RBME.2019.2939091

[11] Ottacher, D., Chan, A., Parent, E., Lou, E.: Positional and orientational accuracy of 3-d ultrasound navigation system on vertebral phantom study. IEEE Trans Instrum Meas **69**(9), 6412–6419 (2020). https://doi.org/10.1109/TIM.2020.2973839

[12] Chan, A., Parent, E., Mahood, J., Lou, E.: 3d ultrasound navigation system for screw insertion in posterior spine surgery: a phantom study. Int. J. Comput. Assist. Radiol. Surg. **17**(2), 271–281 (2022). https://doi.org/10.1007/s11548-021-02516-9

[13] Roshan, M.C., Pranata, A., Isaksson, M.: Robotic ultrasonography for autonomous non-invasive diagnosis—a systematic literature review. IEEE Transactions on Medical Robotics and Bionics **4**(4), 863–874 (2022). https://doi.org/10.1109/TMRB.2022.3201651

[14] Tan, J., Li, B., Leng, Y., Li, Y., Peng, J., Wu, J., Luo, B., Chen, X., Rong, Y., Fu, C.: Fully automatic dual-probe lung ultrasound scanning robot for screening triage. IEEE Transactions on Ultrasonics, Ferroelectrics, and Frequency Control (2022). https://doi.org/10.1109/TUFFC.2022.3211532

[15] Li, R., Davoodi, A., Cai, Y., Niu, K., Borghesan, G., Cavalcanti, N., Massalimova, A., Carrillo, F., Laux, C.J., Farshad, M., et al.: Robot-assisted ultrasound reconstruction for spine surgery: from bench-top to pre-clinical study. International journal of computer assisted radiology and surgery, 1–11 (2023). https://doi.org/10.1007/s11548-023-02932-z

[16] Azad, R., Asadi-Aghbolaghi, M., Fathy, M., Escalera, S.: Bi-directional convlstm u-net with densley connected convolutions. In: Proceedings of the IEEE/CVF International Conference on Computer Vision Workshops, pp. 0–0 (2019). https://doi.org/10.1109/ICCVW.2019.00052

[17] Li, R., Cai, Y., Niu, K., Vander Poorten, E.: Comparative quantitative analysis of robotic ultrasound image calibration methods. In: 2021 20th International Conference on Advanced Robotics (ICAR), pp. 511–516 (2021). https://doi.org/10.1109/ICAR53236.2021.9659341

[18] O. Ronneberger, P. Fischer, and T. Brox: U-net: Convolutional networks for biomedical image segmentation. Lecture Notes in Computer Science. **9351**, 234–241 (2015). https://doi.org/arXiv:1505.04597

[19] Sharp, G.C., Lee, S.W., Wehe, D.K.: Icp registration using invariant features. IEEE Trans Pattern Anal Mach Intell **24**(1), 90–102 (2002). https://doi.org/10.1109/34.982886

[20] P. J. Besl and N. D. McKay: A method for registration of 3-d shapes. IEEE Transactions on Pattern Analysis and Machine Intelligence **14**(2), 239–256 (1992). https://doi.org/10.1109/34.121791

[21] Bruyninckx, H.: Open robot control software: the orocos project. In: Proceedings 2001 ICRA. IEEE International Conference on Robotics and Automation (Cat. No.01CH37164), vol. 3, pp. 2523–25283 (2001). https://doi.org/10.1109/ROBOT.2001.933002

[22] Yushkevich, P.A., Gerig, G.: Itk-snap: An intractive medical image segmentation tool to meet the need for expert-guided segmentation of complex medical images. IEEE Pulse **8**(4), 54–57 (2017). https://doi.org/10.1109/MPUL.2017.2701493

[23] Li, R., Niu, K., Vander Poorten, E.: A framework for fast automatic robot ultrasound calibration. In: 2021 International Symposium on Medical Robotics (ISMR), pp. 1–7 (2021). https://doi.org/10.1109/ISMR48346.2021.9661495

[24] Vörös, V., Li, R., Davoodi, A., Wybaillie, G., Vander Poorten, E., Niu, K.: An augmented reality-based interaction scheme for robotic pedicle screw placement. Journal of Imaging **8**(10), 273 (2022). https://doi.org/10.3390/jimaging8100273

[25] Malham, G.M., Munday, N.R.: Comparison of novel machine vision spinal image guidance system with existing 3d fluoroscopy-based navigation system:

a randomized prospective study. The Spine Journal **22**(4), 561–569 (2022). https://doi.org/10.1016/j.spinee.2021.10.002

[26] Burström, G., Balicki, M., Patriciu, A., Kyne, S., Popovic, A., Holthuizen, R., Homan, R., Skulason, H., Persson, O., Edström, E., *et al.*: Feasibility and accuracy of a robotic guidance system for navigated spine surgery in a hybrid operating room: a cadaver study. Scientific Reports **10**(1), 1–9 (2020). https://doi.org/10.1038/s41598-020-64462-x

[27] Pandey, P.U., Quader, N., Guy, P., Garbi, R., Hodgson, A.J.: Ultrasound bone segmentation: A scoping review of techniques and validation practices. Ultrasound in Medicine & Biology **46**(4), 921–935 (2020). https://doi.org/10.1016/j.ultrasmedbio.2019.12.014.

[28] Victorova, M., Lau, H.H.T., Lee, T.T.-Y., Navarro-Alarcon, D., Zheng, Y.: Comparison of ultrasound scanning for scoliosis assessment: Robotic versus manual. The International Journal of Medical Robotics and Computer Assisted Surgery **19**(2), 2468 (2023). https://doi.org/10.1002/rcs.2468

[29] Sarkar, A., Santiago, R.J., Smith, R., Kassaee, A.: Comparison of manual vs. automated multimodality (ct-mri) image registration for brain tumors. Medical Dosimetry **30**(1), 20–24 (2005). https://doi.org/10.1016/j.meddos.2004.10.004

[30] Korsager, A.S., Carl, J., Østergaard, L.R.: Comparison of manual and automatic mr-ct registration for radiotherapy of prostate cancer. Journal of applied clinical medical physics **17**(3), 294–303 (2016). https://doi.org/10.1120/jacmp.v17i3.6088

[31] Wein, W., Karamalis, A., Baumgartner, A., Navab, N.: Automatic bone detection and soft tissue aware ultrasound–ct registration for computer-aided orthopedic surgery. Int J Comput Assist Radiol Surg **10**, 971–979 (2015). https://doi.org/10.1007/s11548-015-1208-z

[32] Salehi, M., Prevost, R., Moctezuma, J.-L., Navab, N., Wein, W.: Precise ultrasound bone registration with learning-based segmentation and speed of sound calibration. In: Medical Image Computing and Computer-Assisted Intervention-MICCAI 2017: 20th International Conference, Quebec City, QC, Canada, September 11-13, 2017, Proceedings, Part II 20, pp. 682–690 (2017). https://doi.org/10.1007/978-3-319-66185-8_77. Springer

[33] Brößner, P., Hohlmann, B., Welle, K., Radermacher, K.: Ultrasound-based registration for the computer-assisted navigated percutaneous scaphoid fixation. IEEE Transactions on Ultrasonics, Ferroelectrics, and Frequency Control (2023). https://doi.org/10.1109/TUFFC.2023.3291387